ACS APPLIED MATERIALS & INTERFACES

Research Article

www.acsami.org

Low-Temperature Crystalline Titanium Dioxide by Atomic Layer Deposition for Dye-Sensitized Solar Cells

Aravind Kumar Chandiran, Aswani Yella, Morgan Stefik, Leo-Philipp Heiniger, Pascal Comte, Mohammad. K. Nazeeruddin,* and Michael Grätzel*

Laboratory of Photonics and Interfaces, Institute of Chemical Sciences and Engineering, Swiss Federal Institute of Technology (EPFL), Station 6, 1015 Lausanne, Switzerland

Supporting Information

ABSTRACT: Low-temperature processing of dye-sensitized solar cells (DSCs) is crucial to enable commercialization with low-cost, plastic substrates. Prior studies have focused on mechanical compression of premade particles on plastic or glass substrates; however, this did not yield sufficient interconnections for good carrier transport. Furthermore, such compression can lead to more heterogeneous porosity. To circumvent these problems, we have developed a low-temperature processing route for photoanodes where crystalline TiO_2 is deposited onto well-defined, mesoporous templates. The TiO_2 is grown by atomic layer deposition (ALD), and the crystalline films are achieved at a growth temperature of 200 °C. The ALD TiO_2 thickness was systematically studied in terms of charge transport and performance to lead to optimized photovoltaic performance. We found that a 15 nm TiO_2 overlayer on an 8 μm thick SiO_2 film leads to a high power conversion efficiency of 7.1% with the state-of-the-art zinc porphyrin sensitizer and cobalt bipyridine redox mediator.

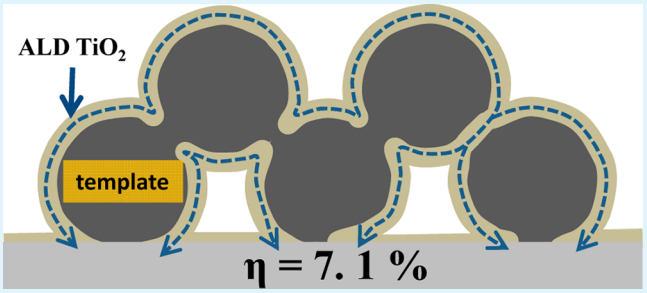

KEYWORDS: *dye-sensitized solar cells, low-temperature titanium dioxide, atomic layer deposition, templates, cobalt complex, flexible solar cell*

INTRODUCTION

Third-generation molecular photovoltaics based on the dye and quantum dot sensitization of the mesoscopic nanostructures have gained attention due to the low cost of manufacturing and ease of fabrication. A typical dye-sensitized solar cell (DSC) is a sandwich of a titanium dioxide photoanode sensitized with dye molecules and a catalyst-coated counter electrode, with a redox electrolyte in-between. The high surface area, porous, and interconnected titanium dioxide nanoparticles serve as a support for the dye sensitizers and transport the photogenerated electrons to the external electrical contact.[1−3] TiO_2 is generally synthesized by a hydrothermal route and made into a paste with polymeric binders which are either screen printed or doctor bladed onto the conducting glass, followed by a high-temperature sintering process at ∼500 °C. The thermal step is carried out to remove the binders and to ensure better electronic contact between particles.[4−6] However, the fabrication of a flexible device on plastic substrates for portable applications requires low-temperature processing. Previously, a low-temperature DSC was made by mechanically compressing the TiO_2 particles or by dispersing the binder free colloidal TiO_2 on the conducting substrates. One of the intrinsic issues with these processing methods is the formation of electronic contact between particles that ensures better charge carrier transport.[7−10] The interfaces between the particles are poorly connected, and hence the percolation of electrons between the particles and to the conducting glass is affected. This issue has been addressed using the atomic layer deposition (ALD) technique by conformally coating TiO_2 onto arbitrary mesoporous templates such as SiO_2, Al_2O_3, fluorine-doped SnO_2, or ZrO_2.[11−15]The conformal coating follows the template morphology, leading to high surface area TiO_2 with continuous pathways for electron transport. Our previous work has shown that a sintered ultrathin 6 nm ALD TiO_2 layer on a mesoporous SiO_2 template is sufficient to effectively transport the photogenerated carriers to the external contacts. The transport rate was found to be 1 order of magnitude higher compared to the standard TiO_2 nanoparticle photoanode films, at a given charge density.[15] Inspired by this study, we extended the work to develop low-temperature crystalline TiO_2 on a similar insulating substrate which can simultaneously possess an undeterred pathway for electrons, unlike other low-temperature routes.[7−10] We report an ALD recipe that leads to crystalline TiO_2 films at a significantly reduced temperature, 200 °C. Films of different thickness were deposited onto the mesoporous SiO_2 substrate, and their photovoltaic performance was studied using our standard D-π-A sensitizer and Co(bipyridine) redox mediator (Figure 1, inset). We find that the as-deposited

Received: March 8, 2013
Accepted: March 18, 2013
Published: March 18, 2013

crystalline films outperformed their sintered counterparts in the photovoltaic performance.

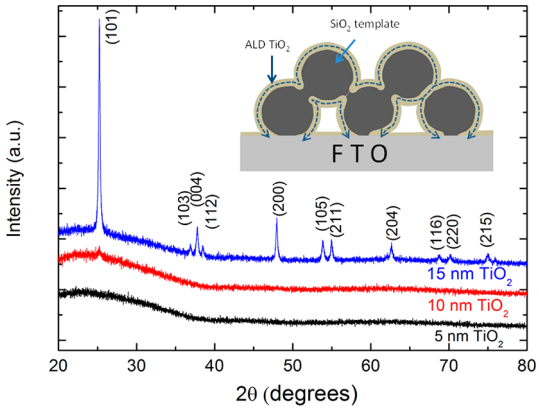

Figure 1. X-ray diffraction patterns of the as-deposited ALD TiO_2 overlayer of three different thicknesses (5, 10, and 15 nm) on 3 μm mesoporous SiO_2 films. The diffraction peaks are assigned to the lattice planes of anatase TiO_2 and are labeled with their Miller indices (*hkl*) (powder diffraction file number 21-1272). The inset schematic depicts the ALD TiO_2 deposited on a silica mesoporous template with the dashed lines indicating the electron transport pathways.

RESULTS AND DISCUSSION

The titanium dioxide was deposited at 200 °C by alternate pulses of titanium isopropoxide (TTIP, 75 °C) and water (25 °C) with an inert gas purge in between.[16] The process of TTIP pulse-purge–H_2O pulse-purge constitutes a single cycle. The thickness of the ALD TiO_2 film was investigated using spectroscopic ellipsometry by depositing 600 cycles on a silicon wafer covered with its native oxide. The obtained data were fitted using a Cauchy dispersion model, and the thickness of the film was found to be 17.9 ± 0.1 nm which gives a growth rate of ~0.03 nm/cycle. To investigate the crystallographic properties of the as-deposited ALD TiO_2, three different thicknesses (5, 10, and 15 nm) of TiO_2 were deposited separately on 3 μm mesoporous SiO_2 films. The growth of TiO_2 on mesoporous silica is similar to that on the Si wafer because the latter is also covered with native SiO_2. However, it has to be noted that the surface acid–base properties might affect the initial growth slightly.[17] When the thickness of the TiO_2 overlayer was less than 10 nm, no specific diffraction pattern related to a crystalline structure was observed. However, a broad peak was detected at low Bragg angles between 20° and 30° which could be due to the presence of uncrystallized residual TiO_2 and the underlying amorphous SiO_2 mesoporous substrate. On increasing the thickness of the overlayer to 15 nm, the diffractogram shows several Bragg reflections, and a comparison with the literature shows that these peaks correspond to titanium dioxide crystallizing in the anatase phase.[5,6] The diffraction patterns for different ALD TiO_2 overlayers and (*hkl*) reflections corresponding to different planes of the anatase crystal lattice are displayed in Figure 1. The above result indicates that when the overlayer reaches a certain critical thickness, between 10 and 15 nm, the crystallization of TiO_2 is initiated. Previously, Aarik et al. have shown that the TiO_2 starts to crystallize at a critical thickness of 15 nm, while the deposition is carried out using $TiCl_4$ and H_2O ALD precursors at 210 °C. However, depending on the substrate, the precursor and temperature of the deposition the critical thickness for crystallization can differ. Yet, in another study by Aarik et al., the TiO_2 film grown using titanium isopropoxide and H_2O is found to crystallize above a critical temperature of 180 °C. Our results on the mesoporous substrates are consistent with these observations on flat substrates.[18,19]

For DSC photoanodes, similar TiO_2 overlayers of 5 and 15 nm were deposited on 3 μm mesoporous SiO_2 films, which were previously screen printed on a transparent conducting glass. The solar cells are made with these as-deposited TiO_2 and also with the similar films sintered at 500 °C, using our standard high molar extinction coefficient organic sensitizer (coded Y123, Figure 2 inset) and cobalt(bipyridine)$_3$ redox

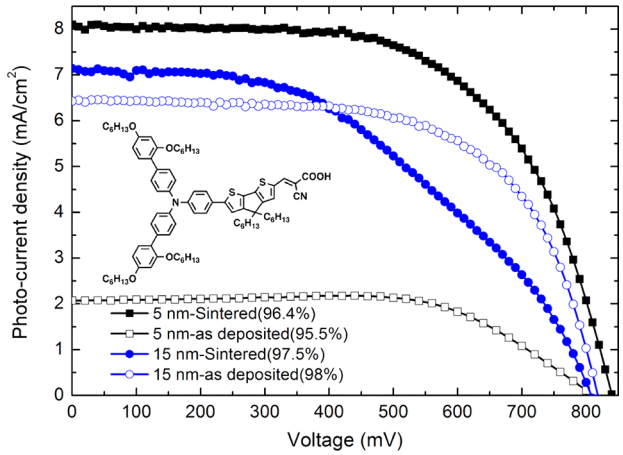

Figure 2. Current–voltage (J–V) characteristics of DSCs with a 5 nm (black squares) and 15 nm (blue circles) TiO_2 overlayer on 3 μm silica films. The numbers in the round brackets (in legends) denote the photon flux under which the J–V measurements are made. The chemical structure shown in the inset is Y123 dye.

mediator.[20] The current–voltage characteristics of the devices are analyzed under standard AM1.5G solar illumination with an intensity equal to 100 mW/cm^2. The mesoporous silica film coated with 5 nm TiO_2 transports a short-circuit current density (J_{SC}) of 2.2 mA/cm^2 with open-circuit potential (V_{OC}) and fill factor (FF) of 809.6 mV and 0.67, respectively, leading to a power conversion efficiency (PCE) of 1.2%, whereas its sintered counterpart could transport 8.5 mA/cm^2 of current, together with an increase of V_{OC} by around 30 mV. The nominal increase of the J_{SC} and V_{OC} overcomes the decline in the fill factor resulting in a PCE of 4.3%. However, when the thickness of TiO_2 is increased to 15 nm, the DSC with the as-deposited film shows remarkably high J_{SC} of 6.6 mA/cm^2, which is 0.8 mA/cm^2 lower than its sintered analogue. The sintering process did not affect the open-circuit potential of the device but exhibits very low fill factor compared to the as-deposited TiO_2 films. Overall the power conversion efficiency of the latter device is higher (3.4% for as-deposited) compared to the 2.7% for the sintered photoanode. The low performance of the 5 nm as-deposited TiO_2 is attributed to the poor transport of the photogenerated electrons in TiO_2 due to its amorphous nature. One has to note that the J_{SC} for the 15 nm sintered TiO_2 is lower than the thinner overlayer (5 nm). This can be explained by the reduction in the available surface area due to the deposition of the thicker overlayer onto the mesoporous substrate as shown previously in ref 15. The dye loading is found to be significantly higher for the 5 nm sintered

TiO_2 film compared to the 15 nm TiO_2 overlayer (Figure S1, Supporting Information) and is consistent with the observed short-circuit current density. The $J-V$ plot and the corresponding data are presented in Figure 2 and Table 1.

Table 1. Short-Circuit Current Density (J_{SC}), Open-Circuit Potential (V_{OC}), Fill Factor (FF), and Power Conversion Efficiency (PCE) of DSCs with Different Thicknesses of the TiO_2 Overlayer on a 3 μm Silica Mesoporous Template

thickness of TiO_2 (nm)	J_{SC} (mA/cm^2)	V_{OC} (mV)	FF	PCE (%)
5/as deposited	2.2	809.6	0.67	1.2
5/sintered	8.5	840.4	0.61	4.3
15/as deposited	6.6	818.2	0.63	3.4
15/sintered	7.4	808.0	0.46	2.7

The incident photon-to-current conversion efficiency (IPCE) is measured for the devices with a 15 nm as-deposited and sintered TiO_2 overlayer. From Figure 3, it can be seen that the

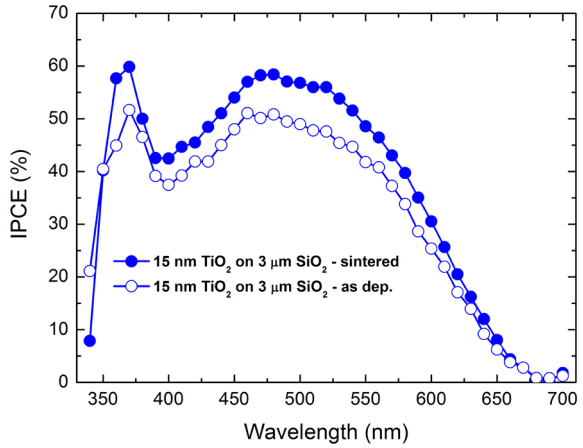

Figure 3. Incident photon-to-electron conversion efficiency of the solar cells containing 15 nm of TiO_2 on 3 μm silica films (sintered, solid circle; as deposited, hollow circle).

onset of the IPCE starts at ~675 nm for both the devices, but the overall IPCE is higher for sintered film which follows the trend of short-circuit current density. The IPCE is determined by the product of four parameters as given in eq 1 below.

$$\mathrm{IPCE} = \Phi_{\mathrm{LHE}} \cdot \Phi_{\mathrm{inj}} \cdot \Phi_{\mathrm{reg}} \cdot \Phi_{\mathrm{coll}} \quad (1)$$

where Φ_{LHE}, Φ_{inj}, Φ_{reg}, and Φ_{coll} are the efficiencies of light harvesting, injection, regeneration, and collection, respectively.[21,22] The following study investigates the aforementioned parameters separately to identify the possible reason for the variation observed in the IPCE between the two devices.

The amount of dye sensitizer adsorbed onto the TiO_2 overlayer before and after sintering is found to be the same within the experimental error (Figure S2, Supporting Information), and hence a change in the IPCE due to the light-harvesting efficiency can be excluded. The second parameter, injection efficiency, is a function of the available driving force for the injection of excited electrons from the LUMO of the dye to the conduction band in TiO_2.[2,23] The dye involved in both devices is Y123, and so the change in LUMO of the dye can be ignored. The electron quasi Fermi level (E_F) is determined by the electronic trap state distribution in the forbidden band gap of the titanium dioxide overlayers. The trap state distribution is measured using a charge extraction technique,[24] and Figure S3 (Supporting Information) shows the plot of voltage as a function of surface defect densities for the sintered (blue solid circle) and the as-deposited (blue hollow circle) films. Similar to the conventional TiO_2 nanoparticles, the trap state profile of ALD TiO_2 shows an exponential increase when moving toward the conduction band from the valence band.[15,23,25] In addition, no change in the distribution is observed in both the sintered and the as-deposited films. Hence for a given electron density in the TiO_2 film, the E_F is expected to be the same, and so in eq 1, the injection efficiency is assumed to be unaltered. Like the first two parameters, the change in the IPCE due to Φ_{reg} can be neglected because the regeneration process is involved between the dye and cobalt complexes and does not depend on the titanium dioxide.

Finally, the collection of the photogenerated electrons in the TiO_2 to the external electrical contact is calculated by measuring the transport rate and recombination rate, respectively, using transient photocurrent and photovoltage decay techniques.[23] The transport rate (Figure 4) of electrons

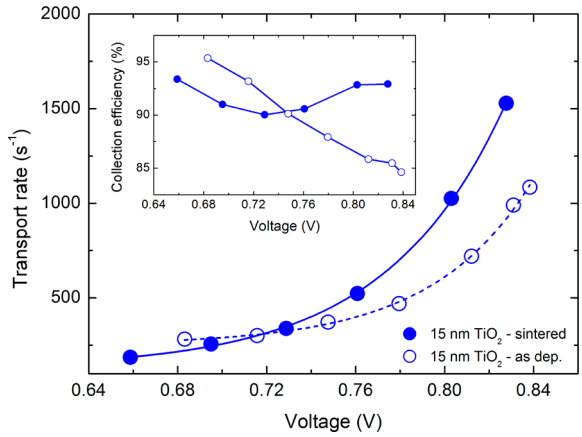

Figure 4. Transport rate of the photogenerated electrons measured as a function of voltage using photocurrent transient decay technique, for 15 nm TiO_2 as-deposited (hollow circle) and sintered (solid circle) photoanodes. Inset shows the collection efficiency of the corresponding devices calculated from the ratio of transport rate to the sum of transport and recombination rate.

in the sintered films is found to be slightly higher for the sintered films (solid circle) as compared to the devices made with the as-deposited (hollow circle) TiO_2. As the distribution of the electronic trap states is found to be similar for both devices, the presence of some proportion of noncrystalline domains in the as-deposited TiO_2 can be attributed to the slow charge percolation along the TiO_2 layer. The presence of larger crystallites in the sintered films also might have contributed to the faster charge transport. The recombination rate (Figure S4, Supporting Information) of electrons from the TiO_2 conduction band to the oxidized redox mediator is found to be unchanged for both the films, which rationalizes the similar open-circuit potential observed in the devices. The last parameter in the IPCE equation, the collection efficiency, is calculated from the ratio of the transport rate to the sum of transport and recombination rate. Figure 4 (inset) shows the calculated Φ_{coll} as a function of voltage. The photoanode sintered at 500 °C shows almost a constant current collection (>90%) over the range of voltages, whereas the device made

dx.doi.org/10.1021/am400866s | ACS Appl. Mater. Interfaces 2013, 5, 3487−3493

with the as-deposited TiO_2 exhibits a decreasing trend. At the operating voltages, the charge collection for the latter is less than the former.[2,23,26] Therefore, the trend observed in the IPCE originates from the variation in the collection efficiency of the photogenarated electrons for the device containing as-deposited and sintered TiO_2 overlayers. The decrease in the fill factor of the devices observed with the sintered films is attributed to the higher photocurrent increasing the Ohmic losses by the same factor.

In the devices described above, the efficiencies are low due to thin photoanodes (3 μm SiO_2). To improve the light harvesting, we extended the thickness of the silica mesoporous template to 8 and 12 μm. A 15 nm TiO_2 layer was deposited on these silica templates, and the photovoltaic properties of the as-deposited films were investigated. The $J-V$ curves and the corresponding photovoltaic data are presented in Figure 5 and

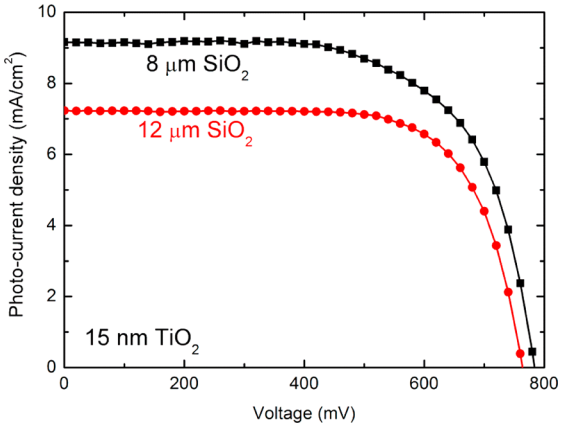

Figure 5. $J-V$ characteristics of solar cells with an as-deposited 15 nm TiO_2 overlayer on 8 μm (black squares) and 12 μm (red circles) silica films measured under AM 1.5 Global sun illumination conditions.

Table 2. Photovoltaic Properties of DSCs with an As-Deposited 15 nm TiO_2 Overlayer on 8 and 12 μm Silica Films

thickness of SiO_2 (μm)	J_{SC} (mA/cm^2)	V_{OC} (mV)	FF	PCE (%)
8	9.2	783.3	0.65	4.7
12	7.2	762.0	0.71	3.9

Table 2, respectively. The 8 μm SiO_2 film gives a photocurrent density of 9.2 mA/cm^2 which is 2.6 mA/cm^2 higher than the 3 μm film, and it is coupled with a slight increase in the fill factor of the device. However, a 15 nm ALD TiO_2 overlayer on 12 μm silica shows a decrease in the J_{SC} to 7.2 mA/cm^2. This decrease might come from nonuniform deposition of the TiO_2 into the higher aspect ratio pores of the thicker silica film. The IPCEs of the corresponding devices are displayed in Figure S5 (Supporting Information). The silica templates utilized had an average pore diameter of 60 nm, leading to an aspect ratio of 200 for a 12 μm thick template. ALD is capable of depositing conformal film on structures having an aspect ratio over 1000.[27,28] However, the particular combination of precursors, the pore morphology, and pore size also affect the accessible aspect ratios. Thus, it can be said that the TTIP could not uniformly diffuse deep into the 12 μm film. To evidence the nonuniformity, we carried out a microscopic investigation on the powders scratched from the TiO_2-on-12 μm SiO_2 film. 333 cycles of TiO_2 were deposited, corresponding to 10 nm TiO_2, as determined by spectroscopic ellipsometry. The TEM micrographs shown in Figure 6A and Figure S6 (Supporting Information) show that the thickness of the overlayer is around 10 nm which is consistent with the ellipsometric data. However, we also observed that some silica particles possess TiO_2 ALD layers greater (denoted as 2 in Figure 6B) and less (denoted as 1 in Figure 6B) than 10 nm. This nonuniformity probably results from the low diffusivity of TTIP precursors along the 12 μm mesoporous SiO_2 film.

A photocurrent transient is measured at different sunlight intensities to further investigate the nonuniform deposition of the TiO_2 (Figure 7). The solid lines show the current density observed at different illumination levels (numbers in red), and they are normalized to one sun photon flux (dotted lines). The normalized current at 9.7% sun predicts that, at 1 sun, the expected current density is around ~8.5 mA/cm^2, but the experimentally observed value is ~7 mA/cm^2. With increasing illumination intensity, the predicted maximum value for 1 sun decreases progressively. This might be due to a thinner TiO_2 layer close to the FTO that restricts current flow. However, the latter device could transport a current density of ~7 mA/cm^2. This result suggests that during the first few nanometers of TiO_2 deposition the precursors diffuse completely into the film, but beyond a certain coating thickness either the metal or oxidizing or both the precursors could not penetrate down to the FTO due to the reduction in the pore diameter. This leads to a gradient in the thickness of the TiO_2 overlayer, through the SiO_2 film. The presence of thinner TiO_2 layers (on SiO_2) closer to FTO limits the transport of charges and can be a reason for the progressive decrease of the normalized current density shown in Figure 7. However, the clogging of pores can be ruled out as a constant current density is observed during a certain illumination time (denoted as ON and OFF in Figure 7) in the transient measurement.[29−31] If there exists a clogging or narrowing of pores, the shuttling of redox systems between the photoanode and counter electrode in the small pores (pore diameter <20 nm) can be restricted at higher current densities which results in a decrease in the current transient with time. From these optimizations, we found the best performance from a 15 nm as-deposited TiO_2 overlayer on 8 μm mesoporous SiO_2.

Finally, we employed the aforementioned optimized photoanode in a DSC with the state-of-the-art highly efficient Zn-porphyrin sensitizer (coded YD-*O*-C8, Figure 8 inset) and a carbon counter electrode to reach a power conversion efficiency of 7.1% with J_{SC} = 10.6 mA/cm^2, V_{OC} = 942.5 mV, and FF = 0.71. The $J-V$ plot of the device is shown in Figure 8.[22,32,33] The IPCE of the corresponding device is shown in Figure S7 (Supporting Information).

CONCLUSION

Many prior approaches to low-temperature DSC photoanode preparation have been limited to low power conversion efficiencies due to the poor particle interconnections. We have demonstrated a new low-temperature technique for photoanode preparation with improved electronic interconnections for efficient charge percolation as shown in Figure 1 (inset). Photoanodes were fabricated by ALD of crystalline TiO_2 onto mesoporous silica templates. The resulting anatase films were mesoporous and continuous, providing a high surface area with continuous percolation paths for charge

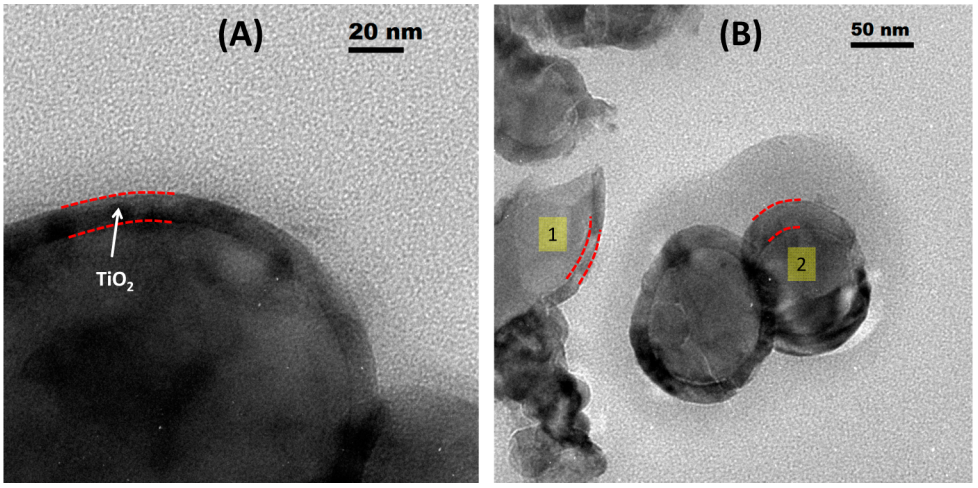

Figure 6. TEM micrographs of the TiO_2 ALD overlayer deposited on a 12 μm mesoporous SiO_2 film. (A) 10 nm TiO_2. (B) Deviation of the thickness from the expected 10 nm TiO_2; the layer thinner than 10 nm is denoted as 1 and thicker as 2.

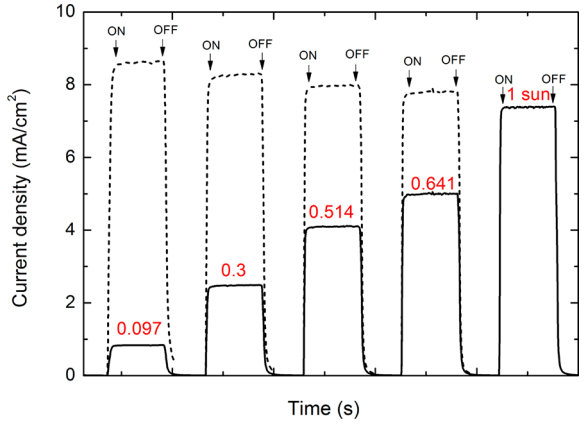

Figure 7. Photocurrent transient (solid line) measured at different light intensities (in red) for the solar cell with an as-deposited 15 nm TiO_2 overlayer on a 12 μm SiO_2 photoanode film. The current densities normalized to 1 sun illumination are denoted with dotted lines.

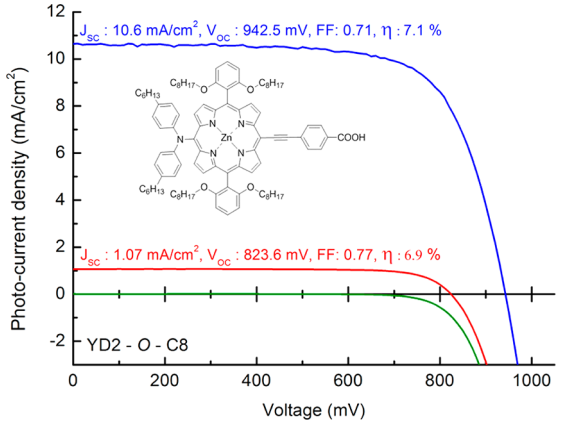

Figure 8. Photovoltaic performance of the DSC containing 15 nm TiO_2 on 8 μm SiO_2 sensitized with YD2-*O*-C8 (chemical structure in the inset) at different illumination levels (blue, 1 sun; red, 0.1 sun; green, dark current).

collection. A minimum TiO_2 thickness of 15 nm was needed to obtain crystalline films. This new approach enabled a high power conversion efficiency of 7.1% with a porphyrin sensitizer. The ALD approach presented here is generalizable to a number of arbitrary templates for low-temperature photoanode fabrication. We anticipate that new ALD protocols and different oxides will enable ALD fabrication of crystalline DSC photoanodes at yet lower temperatures.

METHODS

Preparation of Mesoporous Silica on TCO. The solvents and reagents used in this work are of puriss grade. Unless otherwise mentioned, the materials are used as received without further purification. The hydrophilic fumed SiO_2 (aerosol 90, Evonik Industrie AG, Germany) is made into a screen printable paste using ethyl cellulose of two different viscosities and terpineol, following the procedure similar to the TiO_2 paste preparation described in the literature.[4−6] From the N_2 physisorption measurements, the mean particle size was found to be 28 nm with a pore diameter and porosity of 60 nm and 80%, respectively. The paste was screen printed onto a precleaned TCO glass (NSG 10, Nippon sheet glass, Japan) followed by a series of sintering steps (125 °C for 10 min with ramp time 5 min, 325 °C for 5 min with 15 min ramp time, 375 °C for 5 min with 5 min ramp time, 450 °C for 15 min with 5 min ramp time, and 500 °C for 15 min with 5 min ramp time), and the sintered films were used for the deposition of TiO_2 by ALD. The thickness of the printed film after sintering was measured using a KLA Tencor alpha-step 500 surface profilometer. Please note that template selection is flexible and does not necessarily require a calcination step.

ALD of TiO_2. The deposition of titanium dioxide on the screen printed mesoporous silicon dioxide template is achieved using an atomic layer deposition (ALD) instrument (Cambridge Nanotech Savannah S100). The deposition was carried out using successive pulses of titanium isopropoxide (TTIP, 75 °C) and deionized water (PureLab Analytic ELGA, 18.2 MΩ·cm, 25 °C) using nitrogen as a carrier gas (5 sccm). Following the 100 ms TTIP or 10 ms H_2O pulse, the precursors are confined inside the ALD reactor for 30 s (exposure time) to ensure a complete exposure inside the mesopores of photoanode. Up to 500 cycles of deposition were carried out on SiO_2 substrates and used as photoanodes for DSCs. Both the as-deposited films and the films sintered at 500 °C are used in the study.[34]

Material Characterization. TiO_2 overlayer morphology was studied using a Philips/FEI CM12 TEM equipped with a LaB6 source and operated at 120 kV accelerating voltage. Bright-field images were recorded with a multiscan CCD camera (Gatan). The thickness of the ALD titania layer was evaluated using spectroscopic ellipsometry by depositing a similar number of cycles with identical growth conditions on Si wafers having native oxide. The range of photon energies used in the study is between 1.5 and 5.5 eV (Sopra GES 5E). The obtained spectra were fitted using modified-Cauchy dispersion

dx.doi.org/10.1021/am400866s | ACS Appl. Mater. Interfaces 2013, 5, 3487−3493

law (using WinELI software) to extract the thickness of the deposited TiO_2 layers. The crystallographic properties of the TiO_2 deposited on mesoporous SiO_2 were investigated by X-ray diffraction with a Bruker D8 Discover apparatus. For this study, the mesoporous silica films were prepared on a microscopic slide followed by the deposition of different thicknesses of ALD TiO_2. The instrument is set in "locked coupled' mode, and the acquisition is made for every 0.1° increment over the range of 20° to 80° Bragg angle. The dye loading is measured by desorbing the adsorbed dye in DMF containing basic salt using an HP spectrophotometer (model: HP 8453).

DSC Assembly. The ALD TiO_2 overlayer of different thicknesses (5 and 15 nm) on a mesoporous SiO_2 substrate was used as photoanodes with and without sintering. The photoanodes with the as-deposited TiO_2 overlayer are treated in O_2 plasma (model: PDC-32G, Harrick Plasma, USA) for 5 min before dipping them in the 0.1 mM dye solution in a 50/50 (v/v) acetonitrile/*t*-butanol mixture for 8 h. Similar films sintered at 500 °C (30 min) were also used for comparison. The dyes used in this study are Y123 dye (Figure 2 inset) and YD-*O*-C8 dye (Figure 8 inset). The synthetic procedures of the dyes and the $[Co^{II}(bpy)_3](PF_6)_2/[Co^{III}(bpy)_3](PF_6)_3$ (redox potential = 0.56 V vs NHE) redox mediators are described elsewhere.[20,22] The sensitized electrodes were then washed in acetonitrile to remove the loosely bound dye molecule aggregates before the cell assembly. The counter electrode was made either (a) by thermally depositing Pt at 410 °C for 20 min from a 5 mM H_2PtCl_6 (Aldrich, Germany) ethanolic solution or (b) by depositing ethanolic solution of carbon (stacked graphene platelet nanofiber (acid washed) ABCR, Germany) on the FTO glass (TEC7, Solaronix, Switzerland). The two electrodes were melt sealed using a 25 μm thick Surlyn (Dupont, USA) polymer film. The electrolyte used was a mixture of 200 mM Co^{2+}, 50 mM Co^{3+}, 100 mM $LiClO_4$, and 200 mM *tert*-butyl pyridine in acetonitrile solvent. The electrolyte was injected by a vacuum backfilling technique through a hole sand blasted at the backside of the counter electrodes.

Photovoltaic Characterization. A 450 W xenon lamp (Oriel, USA) was used as a solar simulator for photovoltaic ($J-V$) characterizations. The spectral output of the lamp was filtered using a Schott K113 Tempax sunlight filter (Präzisions Glas & Optik GmbH, Germany) to reduce the mismatch between the simulated and actual solar spectrum to less than 2%. The $J-V$ characteristics of the cells were recorded with a Keithley model 2400 digital source meter (Keithley, USA). The photoactive area of 0.159 cm^2 was defined using a blackened metal mask. Incident photon-to-current conversion efficiency measurements were determined using a 300 W xenon light source (ILC Technology, USA). A Gemini-180 double monochromator Jobin Yvon Ltd. (UK) was used to select and increment the wavelength of the radiation impinging on the cells. The monochromatic incident light was passed through a chopper running at 1 Hz frequency, and the on/off ratio was measured by an operational amplifier. This was superimposed on a white light bias corresponding to 5 mW/cm^2 intensity. The electron transport and recombination in the mesoporous film were measured by transient photocurrent and photovoltage decay measurements, respectively. The white light was generated by an array of LEDs, while a pulsed red light (0.05 s square pulse width) was controlled by a fast solid-state switch to ascertain rapid submillisecond rise of light perturbation. The electrical data were recorded on a mac-interfaced Keithley 2602 source meter.

■ ASSOCIATED CONTENT

Supporting Information

Visible absorption spectra of photoanodes, surface trap states distribution, and recombination rate of 15 nm TiO_2 on SiO_2 before and after sintering; IPCE plot of 15 nm TiO_2 on 8 and 12 μm SiO_2 with Y123 dye; and TEM micrographs of the TiO_2 overlayer on SiO_2 and IPCE of the 15 nm TiO_2 on 8 μm SiO_2 with YD2-*O*-C8. This material is available free of charge via the Internet at http://pubs.acs.org.

■ AUTHOR INFORMATION

Corresponding Author

*E-mail: mdkhaja.nazeeruddin@epfl.ch; michael.graetzel@epfl.ch.

Notes

The authors declare no competing financial interest.

■ ACKNOWLEDGMENTS

The authors acknowledge the financial contribution from EU FP7 project "ORION" grant agreement number NMP-229036. We are grateful for the financial support from the Balzan foundation as a part of the 2009 Balzan Prize awarded to Michael Graetzel. This publication is partially based on work supported by the Center for Advanced Molecular Photovoltaics (Award No KUS-C1-015- 21), made by King Abdullah University of Science and Technology (KAUST). MS is grateful for financial support from the Swiss Commission for Technology and Innovation (CTI) (Award No 13369.1 PFFLR-NM).

■ REFERENCES

(1) Grätzel, M. *Nature* **2001**, *414*, 338−344.
(2) Hagfeldt, A.; Boschloo, G.; Sun, L.; Kloo, L.; Pettersson, H. *Chem. Rev.* **2010**, *110*, 6595−6663.
(3) Kamat, P. V. *J. Phys. Chem. C* **2008**, *112*, 18737−18753.
(4) Ito, S.; Murakami, T. N.; Comte, P.; Liska, P.; Grätzel, C.; Nazeeruddin, M. K.; Grätzel, M. *Thin Solid Films* **2008**, *516*, 4613−4619.
(5) Chandiran, A. K.; Sauvage, F.; Casas-Cabanas, M.; Comte, P.; Zakeeruddin, S. M.; Graetzel, M. *J. Phys. Chem. C* **2010**, *114*, 15849−15856.
(6) Chandiran, A. K.; Sauvage, F.; Etgar, L.; Graetzel, M. *J. Phys. Chem. C* **2011**, *115*, 9232−9240.
(7) Lin, L.-Y.; Lee, C.-P.; Tsai, K.-W.; Yeh, M.-H.; Chen, C.-Y.; Vittal, R.; Wu, C.-G.; Ho, K.-C. *Prog. Photovoltaics: Res. Appl.* **2011**, *20*, 181−190.
(8) Grinis, L.; Kotlyar, S.; Rühle, S.; Grinblat, J.; Zaban, A. *Adv. Funct. Mater.* **2009**, *20*, 282−288.
(9) Boschloo, G.; Lindström, H.; Magnusson, E.; Holmberg, A.; Hagfeldt, A. *J. Photochem. Photobiol., A* **2002**, *148*, 11−15.
(10) Lindström, H.; Holmberg, A.; Magnusson, E.; Lindquist, S.-E.; Malmqvist, L.; Hagfeldt, A. *Nano Lett.* **2001**, *1*, 97−100.
(11) Hamann, T. W.; Martinson, A. B. F.; Elam, J. W.; Pellin, M. J.; Hupp, J. T. *J. Phys. Chem. C* **2008**, *112*, 10303−10307.
(12) Li, T. C.; Fabregat-Santiago, F.; Farha, O. K.; Spokoyny, A. M.; Raga, S. R.; Bisquert, J.; Mirkin, C. A.; Marks, T. J.; Hupp, J. T. *J. Phys. Chem. C* **2011**, *115*, 11257−11264.
(13) Yang, Z.; Gao, S.; Li, T.; Liu, F.-Q.; Ren, Y.; Xu, T. *ACS Appl. Mater. Interfaces* **2012**, *4*, 4419−4427.
(14) Martinson, A. B. F.; Elam, J. W.; Liu, J.; Pellin, M. J.; Marks, T. J.; Hupp, J. T. *Nano Lett.* **2008**, *8*, 2862−2866.
(15) Chandiran, A. K.; Comte, P.; Humphry-Baker, R.; Kessler, F.; Yi, C.; Nazeeruddin, M. K.; Grätzel, M. *Adv. Funct. Mater.* **2013**, DOI: 10.1002/adfm.201202956.
(16) Aarik, J.; Aidla, A.; Uustare, T.; Ritala, M.; Leskelä, M. *Appl. Surf. Sci.* **2000**, *161*, 385−395.
(17) Wang, J.; Baroughi, M. F.; Bills, B.; Galipeau, D.; Samadzadeh, R.; Sivoththaman, S. Substrate Dependence of Surface Passivation Using Atomic Layer Deposited Dielectrics. *Photovoltaic Specialists Conference (PVSC), 2009 34th IEEE*, Philadelphia, PA, June 7−12, 2009; pp 001988−001991.
(18) Aarik, J.; Aidla, A.; Uustare, T.; Sammelselg, V. i. *J. Cryst. Growth* **1995**, *148*, 268−275.
(19) Aarik, J.; Aidla, A.; Mändar, H.; Sammelselg, V. i. *J. Cryst. Growth* **2000**, *220*, 531−537.

(20) Tsao, H. N.; Yi, C.; Moehl, T.; Yum, J.-H.; Zakeeruddin, S. M.; Nazeeruddin, M. K.; Grätzel, M. *ChemSusChem* **2011**, *4*, 591−594.
(21) Chandiran, A. K.; Tetreault, N.; Humphry-Baker, R.; Kessler, F.; Baranoff, E.; Yi, C.; Nazeeruddin, M. K.; Grätzel, M. *Nano Lett.* **2012**, *12*, 3941−3947.
(22) Yella, A.; Lee, H.-W.; Tsao, H. N.; Yi, C.; Chandiran, A. K.; Nazeeruddin, M. K.; Diau, E. W.-G.; Yeh, C.-Y.; Zakeeruddin, S. M.; Grätzel, M. *Science* **2011**, *334*, 629−634.
(23) Peter, L. M. *Phys. Chem. Chem. Phys.* **2007**, *9*, 2630−2642.
(24) Duffy, N. W.; Peter, L. M.; Rajapakse, R. M. G.; Wijayantha, K. G. U. *Electrochem. Commun.* **2000**, *2*, 658−662.
(25) Nelson, J.; Haque, S. A.; Klug, D. R.; Durrant, J. R. *Phys. Rev. B* **2001**, *63*, 205321.
(26) O'Regan, B. C.; Durrant, J. R. *Acc. Chem. Res.* **2009**, *42*, 1799−1808.
(27) George, S. M. *Chem. Rev.* **2009**, *110*, 111−131.
(28) Elam, J. W.; Routkevitch, D.; Mardilovich, P. P.; George, S. M. *Chem. Mater.* **2003**, *15*, 3507−3517.
(29) Feldt, S. M.; Gibson, E. A.; Gabrielsson, E.; Sun, L.; Boschloo, G.; Hagfeldt, A. *J. Am. Chem. Soc.* **2010**, *132*, 16714−16724.
(30) Tsao, H. N.; Comte, P.; Yi, C.; Grätzel, M. *ChemPhysChem* **2012**, *13*, 2976−2981.
(31) Nelson, J. J.; Amick, T. J.; Elliott, C. M. *J. Phys. Chem. C* **2008**, *112*, 18255−18263.
(32) Murakami, T. N.; Grätzel, M. *Inorg. Chim. Acta* **2008**, *361*, 572−580.
(33) Murakami, T. N.; Ito, S.; Wang, Q.; Nazeeruddin, M. K.; Bessho, T.; Cesar, I.; Liska, P.; Humphry-Baker, R.; Comte, P.; Péchy, P.; Grätzel, M. *J. Electrochem. Soc.* **2006**, *153*, A2255−A2261.
(34) Leskelä, M.; Ritala, M. *Thin Solid Films* **2002**, *409*, 138−146.